Analysis of Transition Metal Oxides based Heterojunction Solar Cells with S-shaped J-V curves

Scire, Daniele; Bonadonna, Marco; Zhao, Yifeng; Procel , Paul; Isabella, Olindo; Zeman, Miro; Macaluso, Robert; Mosca, Mauro; Crupi, Isodiana

DOI
10.23919/AEIT50178.2020.9241142

Publication date
2020

Document Version
Accepted author manuscript

Published in
12th AEIT International Annual Conference, AEIT 2020

Analysis of Transition Metal Oxides based Heterojunction Solar Cells with S-shaped J-V curves

Daniele Scirè
Dept. of Engineering
University of Palermo
Palermo, Italy
daniele.scire@unipa.it

Marco Bonadonna
Dept. of Engineering
University of Palermo
Palermo, Italy

Yifeng Zhao
Dept. of Electrical Sustainable Energy
Delft University of Technology
Delft, the Netherlands

Paul Procel
Dept. of Electrical Sustainable Energy
Delft University of Technology
Delft, the Netherlands

Olindo Isabella
Dept. of Electrical Sustainable Energy
Delft University of Technology
Delft, the Netherlands

Miro Zeman
Dept. of Electrical Sustainable Energy
Delft University of Technology
Delft, the Netherlands

Roberto Macaluso
Dept. of Engineering
University of Palermo
Palermo, Italy

Mauro Mosca
Dept. of Engineering
University of Palermo
Palermo, Italy

Isodiana Crupi
Dept. of Engineering
University of Palermo
Palermo, Italy

***Abstract*— The use of transition metal oxides for the selective carrier contact in the crystalline silicon solar cells technology is rising to interest for the excellent optoelectrical properties of these materials whose implementation, however, can result in lousy performing cells due to an S-shaped electrical characteristic. In this paper, we fabricated solar cells showing S-shaped J-V curve and carried out an analysis of the reasons of such behavior using a model involving the series of a standard cell equivalent circuit with a Schottky junction in order to explain these atypical performances. A good matching between the experimental measurements and the adopted theoretical model was obtained. The extracted parameters are listed and analyzed to shade light on the reasons behind the low-performance cells.**

Keywords—solar cells, heterojunction, transition metal oxides, pulsed laser deposition, s-shape

I. INTRODUCTION

The photovoltaic market is increasing steadily year by year, leading to a keen interest in the innovation of solar cell technologies [1]. One of the most recent and promising advancements in the field of solar cells is the c-Si (crystalline silicon) HJT (heterojunction technology), which achieved a record efficiency of 26.7% [2]. This solar cell architecture is based on the use of hydrogenated amorphous silicon (a-Si:H) for the passivation and selective carrier contact; such material, however, has some drawbacks associated whit parasitic absorption and large concentrations of defects [3]. Moreover, the passivation properties of a-Si:H can be jeopardized by annealing at temperatures higher than 200°C [4]; therefore, the thermal budget of cells involving this material is limited and the manufacturing steps have to be carried out at lower temperatures.

In this scenario, replacing the doped amorphous silicon with other materials like the transition metal oxides (TMOs), which have excellent transparency (energy gap higher than 3 eV), is a viable alternative [5]. These materials can be deposited with low-temperature processes and can then meet the requirements for being inserted in the overall cells manufacturing process at a reduced cost. Several studies on the use of transition metal oxides for both hole and electron selective contacts have been published and there is interest in further investigation of TMOs-based heterojunction solar cells. In particular, molybdenum trioxide (MoO_3) and tungsten trioxide (WO_3) have been individuated as excellent candidates for the hole selective contact [6], [7].

However, the application of TMOs in HJT is recent compared to amorphous silicon and there is an intense interest in the optimization of solar cells involving such materials [8]. On the other hand, TMO based solar cells can be affected by the formation of S-shaped J–V curves [9], which lead to a considerable decrease in the electrical performances of the cells influencing the fill factor negatively and increasing the losses. For this reason, expanding the knowledge behind the formation mechanisms of the S-shaped current is essential in order to avoid such behavior and further the dissemination of the TMO-based heterojunction technology.

In this paper, we aim to collect information and improve knowledge about the behavior of TMOs in solar cells by applying MoO_3 and WO_3 as selective hole contacts in c-Si HJT. First, we investigated the optical properties of MoO_3 and WO_3 layers deposited on quartz substrates by means of Pulsed Laser Deposition (PLD), a technique that allows obtaining a controllable and reproducible deposition of a broad number of metal oxides [10]–[18]. Then we used the same process to fabricate the TMO-based hole selective contact in solar cell prototypes based on n-type nanocrystalline silicon oxide [19]. After the electrical characterization, we reported S-shaped DC characteristics for all the prototypes. Finally, we used a validated electrical model [20] to fit the DC electrical characteristics and extract the parameters of the equivalent circuit.

XXX-X-XXXX-XXXX-X/XX/$XX.00 ©20XX IEEE

II. Experimental Details

In order to characterize the TMOs optical properties, three MoO_3 and three WO_3 films were deposited by PLD at room temperature (25°C). Commercially available quartz (2 cm × 2 cm) was used as substrates. Before deposition, the substrates were cleaned by ultrasonic bath in acetone for 10 min and then rinsed in isopropyl alcohol and dried up with compressed air. The PLD employed system is described elsewhere [11] and includes a Q-switched tripled Nd:YAG laser (Quantel mod. YG78C20; λ = 355 nm) generating 6 ns width pulses with an energy of 80 mJ per pulse. MO_3 and WO_3 targets (99.9% pure) were both a 1-inch diameter, 0.25-inch thick, sintered MO_3 and WO_3 ceramic disks, respectively. Oxide films were deposited with different oxygen pressures (P_{O2} = 3 × 10^{-2}, 6 × 10^{-2}, 1 × 10^{-1} mbar) to evaluate the influence of this deposition parameter on the optoelectrical properties of the transition metal oxides. The transmittance measurements of such films were carried out in the UV-VIS range using a Varian DMS 90 spectrophotometer system.

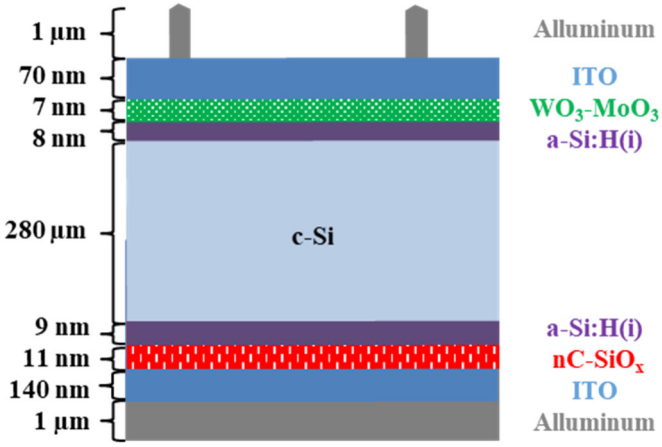

Fig. 1. Sketch of an HJT solar cell with hole selective contact.

The solar cells prototypes were fabricated from a n-type <111> oriented c-Si wafer (thickness = 280 µm, resistivity = 2.5 Ω cm, doping concentration = 1.9 × 10^{15} cm^{-3}). First, the electron contact was formed by PECVD (Plasma Enhanced Chemical Vapor Deposition) with a stack of 8 nm thick a-Si:H(i) passivation layer and then 11 nm of nc-SiOx (n-type nanocrystalline silicon oxide) for the electron selective contact; subsequently, on the other face of the wafer, a passivation layer of 9 nm of a-Si:H(i) was deposited by PECVD.

Afterward, six cell prototypes were obtained by dicing the wafer in squares of 1.5 × 1.5 cm^2 and prepared for the deposition of the hole selective contact. The prototypes were divided into two sets of three cells each: MoO_3 was used in one set while WO_3 for the other one. These layers of TMO were deposited on top of the a-Si:H(i) passivation layer as sketched in Fig. 1 setting the thickness of these layers at 7 nm. Similarly to the films deposited on quartz, P_{O2} of 3 × 10^{-2}, 6 × 10^{-2}, 10 × 10^{-2} mbar were used for the deposition of the oxides onto the solar cell stack in order to study the performances of the cells against different P_{O2} deposition conditions. Finally, the prototypes were finalized by sputtering of indium tin oxide (ITO) as an anti-reflecting coating (70 nm on the front side, 140 nm on the back side) while metallization was obtained by thermal evaporation of 1 µm-thick aluminum on both faces of the devices. In particular, the bottom contact was obtained with a plan Al deposition onto the nc-SiOx film, whilst the top contact, having a grid pattern, was deposited onto the ITO film through a shadow mask. A photo of the final device is presented in Fig. 2; the area of the completed cell is 1 cm^2.

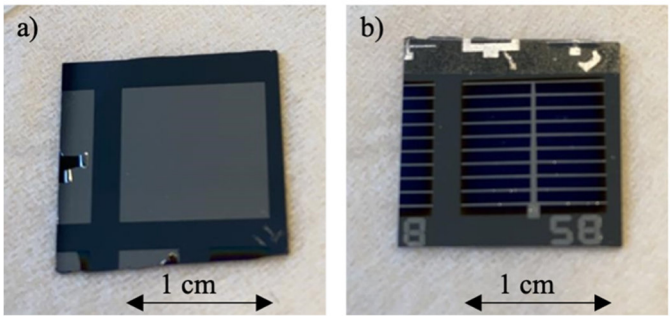

Fig. 2. Solar cell prototype: a) back contact, b) top contact.

The current density–voltage (J–V) characteristics of the devices were measured with a source-meter under standard test condition (STC: 1 sun, T_{CELL} 25°C, air mass 1.5).

III. OptoElectrical Characterization

A. Film characterization

The optical properties of the TMOs were evaluated from the samples grown by PLD on quartz. The transmission spectra of the MoO_3 samples, presented in Fig. 3, show that the material absorbs most of the light in the 200-350 nm range and is transparent for higher wavelengths. Moreover, the transmissivity depends on the P_{O2}: the higher is the oxygen pressure, the higher is the film transmittivity. A similar trend can also be noted in Fig. 4 for the tungsten oxide samples: it is opaque in the 200-310 nm range and then transparent for higher wavelengths; also in this case, the highest transmittivity values are obtained with the highest oxygen pressures.

From the transmissivity data is also possible to evaluate optical bandgap (E_G) of the material through the linear regression of the Tauc's relation [21] reported in the following equation :

$$(\alpha h\nu)^n = B\,(h\nu - E_G) \qquad (1)$$

where α is the absorption coefficient (calculated from the transmissivity through the *Lambert-Beer's Law*), $h\nu$ is the energy of the incident photon, n is a material-dependent coefficient, equals to 1/2 for indirect bandgap materials as molybdenum and tungsten oxides [22], [23].

Table I summarizes the optical energy gap data for all the samples. The energy gap is always above 3 eV and the optical energy gap is higher for the samples deposited at the intermediate pressure (6 × 10^{-2} mbar for the WO_3 film and 6 × 10^{-2} mbar for the MoO_3 film). Variations in the optical gap and the transparency of the transition metal oxides are due to the significant presence of oxygen vacancies formed during the deposition; in particular, a low oxygen pressure during deposition enhances this phenomenon. For this reason, the films are sub-stoichiometric (MoO_x and WO_x with x approaching 3).

This characterization underlines the remarkable optical properties of the deposited transition metal oxides,

highlighting the high transparency for wavelengths higher than 350 nm, making them excellent candidates for the hole selective contact in the heterojunction solar cell technology. Moreover, in comparison with a-Si:H, the transition metal oxides allow achieving a higher optical gap reducing the parasitic absorption.

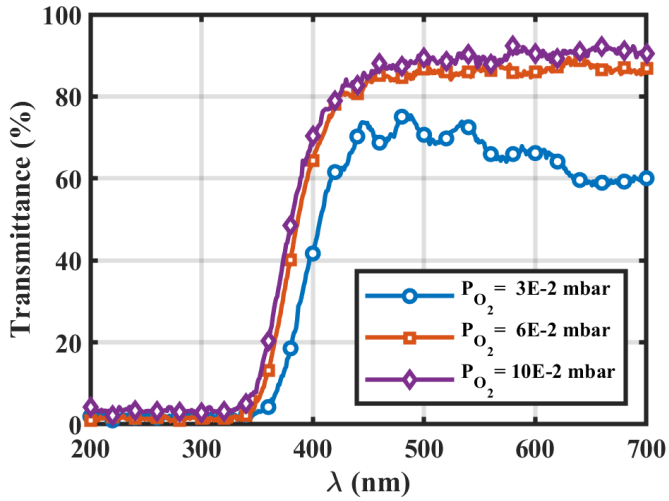

Fig. 3. The transmittance spectra of the MoO_3 films on a quartz substrate against the different deposition oxygen pressures

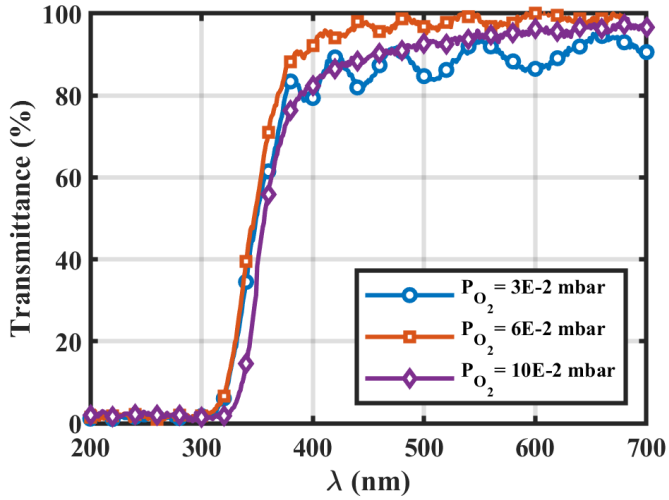

Fig. 4. The transmittance spectra of the WO_3 films on a quartz substrate against the different deposition oxygen pressures

TABLE I. OPTICAL ENERGY GAP

Deposition Oxygen Pressure (mbar)	Optical Band Gap (eV)	
	MoO_3	*WO_3*
3E-2	3.0	3.3
6E-2	3.2	3.4
10E-2	3.0	3.2

B. Solar cell characterization

In Fig. 5 and Fig 6, the experimental J–V curve characteristics under AM 1.5 illumination for the HJT solar cells with MoO_3 or WO_3 as selective carrier contacts are presented.

All the samples showed an S-shaped J-V characteristic. This phenomenon can be associated with a barrier for the extraction of the charge carriers through the introduced TMO films. This barrier is due to the imperfect alignment of the band structure in the cell, between the layers of TMO and the intrinsic hydrogenated amorphous silicon as confirmed by several authors [43,44] and is a limitation in the optimization of the TMO-based solar cells. In fact, the properties of TMOs, such as optical band gap, work function, crystallinity and stoichiometry, depend on the deposition technique as well as the substrate temperature and the deposition oxygen pressure. The variations of these parameters lead to suboptimal electrical DC characteristics. It is worth noting a common trend in the open circuit voltage V_{OC} and the short circuit current density J_{SC} of both materials; in fact, as the oxygen pressure increases both V_{OC} and J_{SC} raise.

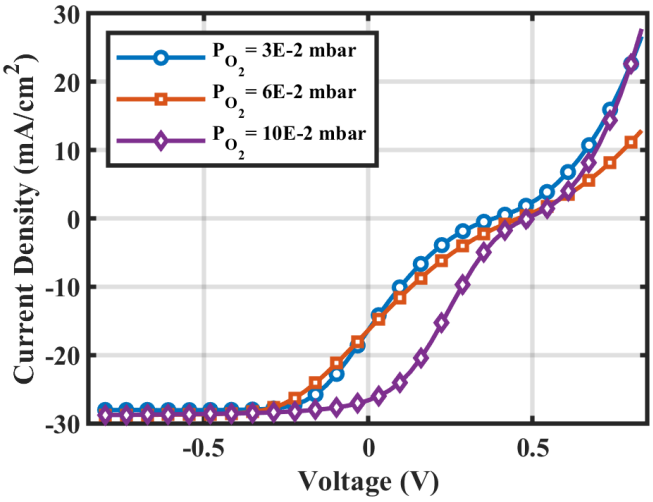

Fig. 5. J-V characteristics of the MoO_3-based heterojunction solar cells against the different oxygen pressures

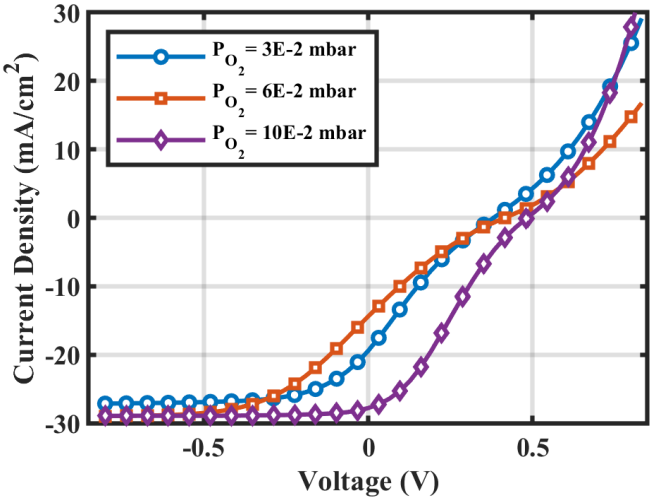

Fig. 6. J-V characteristics of the WO_3-based heterojunction solar cells against the different oxygen pressures

IV. SOLAR CELL PARAMETERS EXTRACTION

A. Theoretical Model

The model of a standard HJT is similar to silicon cells based on p–n junctions but the presence of an S-shape J-V characteristic cannot be explained with this model; as a matter of fact, many examples exist in the literature for modeling cells with an anomalous S-shape DC electrical characteristics

[24]–[26]. In this paper, we adopted the equivalent circuit model (Fig. 7) developed in [20] in which a rectifying junction is connected in series with the heterojunction to model a Schottky barrier.

The heterojunction equivalent cell model is described in equation (2), which includes the exponential diode current, the current loss in the shunt resistance (R_{P1}) and the photogenerated current density (J_{PH}).

$$J = J_{01}\left(exp\left(\frac{V-JR_{S1}-V_1}{n_1V_T}\right)-1\right)+\frac{V-JR_{S1}-V_1}{R_{P1}}-J_{PH} \quad (2)$$

where J is the current density through the solar cell, V is the bias voltage, J_{01} is the leakage current density, n_1 is the ideal factor for the diode of the heterojunction, V_T is the thermal voltage (25.85 mV at 300 K) and R_{S1} is the series resistance.

The Schottky junction is then described by the following equation:

$$J = J_{02}\left(exp\left(\frac{V_1}{n_2V_T}\right)-1\right)+\frac{V_1}{R_{P2}} \quad (3)$$

where J_{02} is the leakage current density, V_1 is the bias voltage of the Schottky junction, n_2 is the ideal factor for the diode.

Equation (3) includes both an exponential diode current and a leakage current terms due to a shunt resistance (R_{P2}). It should be noted that the current density through both heterojunction and Schottky junction is the same, while the overall voltage is split among the junctions.

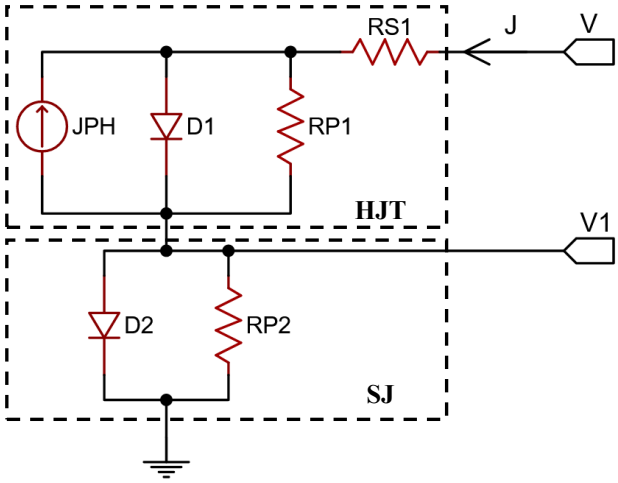

Fig. 7. Equivalent circuit of a heterojunction (HJT) solar cell with a series Schottky junction (SJ)

An expression of the voltage V_1 is needed for the calculation of equation (2); such expression can be obtained through algebraic manipulation in a transcendental form which can be solved numerically i.e. with the Newton-Raphson method. In this work, the *Lambert W* function [27] was used to extract a direct expression of V_1 according to the following equation:

$$V_1 = R_{P2}(J_{02}+J)+n_2V_T\,W\left(\frac{J_{02}R_{P2}}{n_2V_T}exp\left(\frac{R_{P2}(J_{02}+J)}{n_2V_T}\right)\right) \quad (4)$$

where W is the *Lambert W* function.

This method involves a lighter computational load and higher accuracy in comparison to the Newton-Raphson method.

B. Parameters Extraction

Equations (2) and (4) were used to fit the experimental J-V curves of the MoO_3 and WO_3-based solar cells by the minimization of a least-squares problem. By this procedure, quantitative values of the cell parameters were obtained and listed in Table II for the WO_3-based cells and in Table III for the MoO_3 case. The resulting parameters allow a more in-depth analysis and comprehension of the device and its mechanisms. As shown in Figs. 8 and 9, a proper fitting was obtained for the experimental data in the entire voltage range; moreover, a simulation of the J-V curve involving only the heterojunction parameters without the Schottky junction was added for comparison.

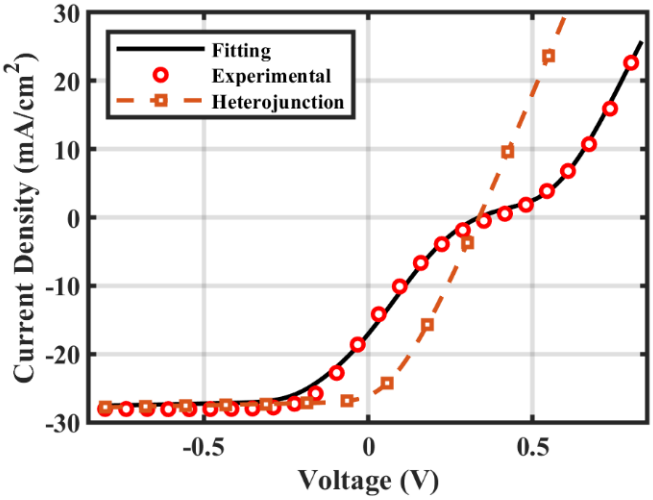

Fig. 8. Fitting of the J-V characteristic of the solar cell with MoO_3 deposited at $P_{O2} = 3 \times 10^{-2}$ mbar.

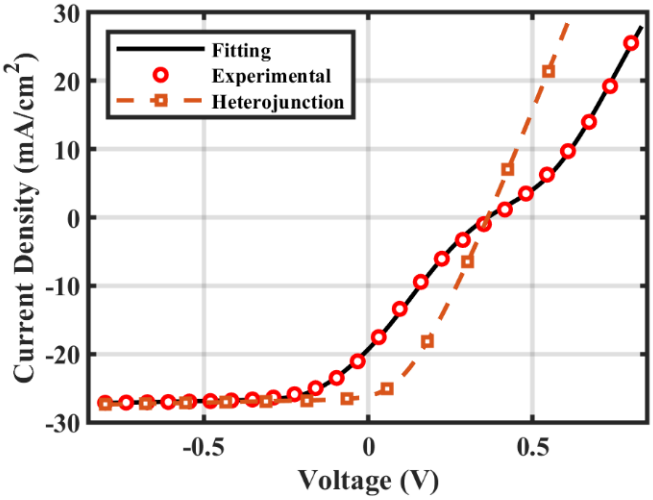

Fig. 9. Fitting of the J-V characteristic of the solar cells with WO_3 deposited at $P_{O2} = 3 \times 10^{-2}$ mbar.

From the comparison of the experimental data with the simulated heterojunction cell, it is possible to highlight several aspects valid for both the TMOs-based cells:

First, the HJT curves and the experimental ones share the same V_{OC}. In fact, when the input voltage reaches the open circuit value, the current density in the whole device is zero

TABLE II. WO_3 SOLAR CELL PARAMETERS

	Heterojunction					Schottky Junction		
Deposition Pressure (mbar)	J_{01} ***(A/cm²)***	R_{S1} ***(Ω·cm²)***	R_{P1} ***(Ω·cm²)***	N_1	J_{PH} ***(A/cm²)***	J_{02} ***(A/cm2)***	R_{P2} ***(Ω·cm²)***	N_2
3E-2	3.6E-6	7.5	1000	1.6	2.68E-02	1.35E-04	8.5	2.7
6E-2	1.7E-6	11.2	1000	1.6	2.88E-02	9.25E-05	12.0	2.7
10E-2	6.3E-7	4.7	1000	1.6	2.87E-02	3.68E-04	6.0	2.6

TABLE III. MoO_3 SOLAR CELL PARAMETERS

	Heterojunction					Schottky Junction		
Deposition Pressure (mbar)	J_{01} ***(A/cm²)***	R_{S1} ***(Ω·cm²)***	R_{P1} ***(Ω·cm²)***	N_1	J_{PH} ***(A/cm²)***	J_{02} ***(A/cm²)***	R_{P2} ***(Ω·cm²)***	N_2
3E-2	4.7E-06	7.9	1000	1.5	2.7E-02	6.4E-05	8.9	2.7
6E-2	3.5E-07	10.9	1000	1.5	2.9E-02	4.8E-05	11.6	2.7
10E-2	3.9E-07	5.4	1000	1.6	2.8E-02	2.5E-04	6.7	2.7

and the entire bias voltage is then applied at the top section of the circuit model (Fig. 7) implying that the Schottky junction is not involved in the determination of the V_{OC}. Moreover, the open-circuit voltage grows as the deposition pressure raises, meaning that the devices with the higher oxygen deposition pressure have the lowest recombination losses. It is worth noting that the V_{OC} depends on the saturation current density J_{01} whose values were extracted through the fitting, and exhibit a descending trend as the P_{O2} raises. This applies for both the MoO_3 and WO_3 cells.

Second, the slope in the DC characteristic near the open-circuit voltage depends on the differential conductance of the device. This value is dominated by the Schottky barrier conductance at the open-circuit voltage ($1/R_{P2}$), which is much lower than the differential conductance of the heterojunction ($1/R_{P1}$). For this reason, the slope of the characteristic changes at around V_{OC} forming the S-shaped curve. When the bias voltage further increases, D_2 enters in conduction shortening R_{P2} and the J-V curve slope is now equal to $1/R_{P1}$ as in the HJT simulated cell. The Schottky barrier causes a shift of the J-V curve toward higher voltage with respect to the simulated heterojunction cell; in fact, D_2 increases the forward turn-on voltage of the cell.

Finally, for bias voltage smaller than V_{OC}, the Schottky junction is reversely biased, which represents an obstacle for the charge transport through the device. Due to this, current density of the prototypes, at a parity of voltage, is lower than the corresponding HJT cells resulting in a lower fill factor. As the bias voltage further decreases, the photogenerated current density is dominant and J reaches its minimum value, which is equal to the HJT simulated one.

V. CONCLUSIONS

MO_3 and WO_3 transition metal oxides films were first deposited onto quartz substrates, and then optically characterized. The impact of these materials as selective carrier contacts in c-Si heterojunction solar cells was successively tested by realizing a set of prototypes with TMOs deposited at different oxygen pressures. Afterward, the fabricated cells were electrically characterized and all the devices exhibited an S-shaped DC J-V curve. The behavior of these cells was analyzed by the implementation of a model previously developed for solar cells presenting anomalous electrical characteristics. The experimental data were used to determine a quantitative parameter for the solar cell equivalent parameters. The simulated characteristics resulted in a good fit with the measured data for a broad voltage range. The results show the potential of the TMO-based c-Si HJT and giving input for further optimization of the MoO_3 and WO_3-based cells.

REFERENCES

[1] P. K. Nayak, S. Mahesh, H. J. Snaith, and D. Cahen, "Photovoltaic solar cell technologies: analyzing the state of the art," *Nat. Rev. Mater.*, 2019.

[2] M. A. Green, E. D. Dunlop, J. Hohl-Ebinger, M. Yoshita, N. Kopidakis, and A. W. Y. Ho-Baillie, "Solar cell efficiency tables (Version 55)," *Prog. Photovoltaics Res. Appl.*, vol. 28, no. 1, pp. 3–15, 2020.

[3] Z. C. Holman *et al.*, "Current Losses at the Front of Silicon Heterojunction Solar Cells," *IEEE J. Photovoltaics*, vol. 2, no. 1, pp. 7–15, Jan. 2012.

[4] B. Macco *et al.*, "Correlating the silicon surface passivation to the nanostructure of low-temperature a-Si:H after rapid thermal annealing," *J. Appl. Phys.*, 2017.

[5] J. Melskens, B. W. H. Van De Loo, B. Macco, L. E. Black, S. Smit, and W. M. M. Kessels, "Passivating Contacts for Crystalline Silicon Solar Cells: From Concepts and Materials to Prospects," *IEEE J. Photovoltaics*, vol. 8, no. 2, pp. 373–388, 2018.

[6] C. Battaglia *et al.*, "Hole selective MoOx contact for silicon solar cells," *Nano Lett.*, vol. 14, no. 2, pp. 967–971, Feb. 2014.

[7] M. Bivour, J. Temmler, H. Steinkemper, and M. Hermle, "Molybdenum and tungsten oxide: High work function wide band gap contact materials for hole selective contacts of silicon solar cells," *Sol. Energy Mater. Sol. Cells*, vol. 142, pp. 34–41, 2015.

[8] R. A. Vijayan *et al.*, "Hole-Collection Mechanism in Passivating Metal-Oxide Contacts on Si Solar Cells: Insights from Numerical Simulations," *IEEE J. Photovoltaics*, vol. 8, no. 2, pp. 473–482, 2018.

[9] C. Messmer, M. Bivour, J. Schön, and M. Hermle, "Requirements for efficient hole extraction in transition metal oxide-based silicon heterojunction solar cells," *J. Appl. Phys.*, 2018.

[10] T. Cesca *et al.*, "Correlation between in situ structural and optical characterization of the semiconductor-to-metal phase transition of VO2 thin films on sapphire," *Nanoscale*, vol. 12, no. 2, pp. 851–863, 2020.

[11] A. Boughelout, R. Macaluso, I. Crupi, B. Megna, M. S. Aida, and M. Kechouane, "Improved Cu2O/AZO Heterojunction by Inserting a Thin ZnO Interlayer Grown by Pulsed Laser Deposition," *J. Electron. Mater.*, vol. 48, no. 7, pp. 4381–4388, 2019.

[12] A. Boughelout, R. Macaluso, M. Kechouane, and M. Trari, "Photocatalysis of rhodamine B and methyl orange degradation under solar light on ZnO and Cu2O thin films," *React. Kinet. Mech. Catal.*, vol. 129, no. 2, pp. 1115–1130, 2020.

[13] M. Barbouche *et al.*, "New process of silicon carbide purification intended for silicon passivation," *Superlattices Microstruct.*, vol. 101, pp. 512–521, 2017.

[14] A. Sacco *et al.*, "Enhancement of photoconversion efficiency in dye-sensitized solar cells exploiting pulsed laser deposited niobium pentoxide blocking layers," *Thin Solid Films*, vol. 574, pp. 38–42, 2015.

[15] M. Mosca *et al.*, "Optical, structural, and morphological characterisation of epitaxial ZnO films grown by pulsed-laser deposition," *Thin Solid Films*, vol. 539, pp. 55–59, 2013.

[16] R. Macaluso *et al.*, "Erroneous p-type assignment by Hall effect measurements in annealed ZnO films grown on InP substrate," *J. Appl. Phys.*, vol. 113, no. 16, 2013.

[17] C. Calì, R. Macaluso, and M. Mosca, "In situ monitoring of pulsed laser indium-tin-oxide film deposition by optical emission spectroscopy," *Spectrochim. Acta - Part B At. Spectrosc.*, vol. 56, no. 6, pp. 743–751, 2001.

[18] R. Macaluso *et al.*, "Resistive switching behaviour in ZnO and VO2 memristors grown by pulsed laser deposition," *Electron. Lett.*, 2014.

[19] Y. Zhao *et al.*, "Doped hydrogenated nanocrystalline silicon oxide layers for high-efficiency c-Si heterojunction solar cells," *Prog. Photovoltaics Res. Appl.*, vol. 28, no. 5, pp. 425–435, May 2020.

[20] L. Zuo, J. Yao, H. Li, and H. Chen, "Assessing the origin of the S-shaped I-V curve in organic solar cells: An improved equivalent circuit model," *Sol. Energy Mater. Sol. Cells*, 2014.

[21] J. Tauc, R. Grigorovici, and A. Vancu, "Optical Properties and Electronic Structure of Amorphous Germanium," *Phys. status solidi*, vol. 15, no. 2, pp. 627–637, 1966.

[22] K. Inzani, M. Nematollahi, F. Vullum-Bruer, T. Grande, T. W. Reenaas, and S. M. Selbach, "Electronic properties of reduced molybdenum oxides," *Phys. Chem. Chem. Phys.*, vol. 19, no. 13, pp. 9232–9245, 2017.

[23] I. Kostis *et al.*, "Hot-wire substoichiometric tungsten oxide films deposited in hydrogen environment with n-type conductivity," *J. Phys. D. Appl. Phys.*, 2012.

[24] A. Aghassi, C. D. Fay, and A. Mozer, "Investigation of S-shaped current-voltage characteristics in high-performance solution-processed small molecule bulk heterojunction solar cells," *Org. Electron.*, 2018.

[25] F. J. García-Sánchez, D. Lugo-Muñoz, J. Muci, and A. Ortiz-Conde, "Lumped parameter modeling of organic solar cells' S-shaped I-V characteristics," *IEEE J. Photovoltaics*, 2013.

[26] F. J. Garcia-Sanchez and B. Romero, "Equivalent circuit models for next generation photovoltaic devices with s-shaped i-v curves," in *2019 8th International Symposium on Next Generation Electronics, ISNE 2019*, 2019.

[27] R. M. Corless, G. H. Gonnet, D. E. G. Hare, D. J. Jeffrey, and D. E. Knuth, "On the Lambert W function," *Adv. Comput. Math.*, vol. 5, no. 1, pp. 329–359, 1996.